CHEMISTRY OF MATERIALS

Article

pubs.acs.org/cm

Naphtho[2,3-*b*:6,7-*b*′]dichalcogenophenes: Syntheses, Characterizations, and Chalcogene Atom Effects on Organic Field-Effect Transistor and Organic Photovoltaic Devices

Masahiro Nakano,[†,§] Hiroki Mori,[†,§] Shoji Shinamura,[†] and Kazuo Takimiya*[,†,‡]

[†]Department of Applied Chemistry, Graduate School of Engineering, Hiroshima University, Higashi-Hiroshima 739-8527, Japan

[‡]Institute for Advanced Materials Research, Hiroshima University, Higashi-Hiroshima 739-8530, Japan

Supporting Information

ABSTRACT: New linear-shaped naphtho[2,3-*b*:6,7-*b*′]-difurans (NDFs) and -selenophenes (NDSs) were synthesized selectively from 3,7-dibromo-2,6-dihydroxynaphthalene and evaluated as organic semiconductors in comparison to corresponding naphtho[2,3-*b*:6,7-*b*′]dithiophenes (NDTs). Evaluation of the electronic structures of the parent compounds by means of electrochemical and optical measurements clearly indicated that NDT and NDS are quite similar to each other, whereas only NDF has a marked different electronic structure. Thin film devices, including organic field-effect transistors (OFETs) and bilayer photovoltaics (OPVs) with C_{60} or C_{70} as an acceptor layer, were fabricated with the diphenyl derivatives using vacuum deposition. The thin films were found to be nicely crystalline with the edge-on molecular orientation both on Si/SiO_2 (for OFETs) and ITO substrates (for OPVs). The thin films acted as active semiconducting layer in OFETs with mobility higher than 0.1 $cm^2\ V^{-1}\ s^{-1}$ and as a donor layer in OPVs with power conversion efficiencies of up to 2.0%, indicating that the present naphthodichalcogenophenes are potential core structures for the development of new organic semiconductors.

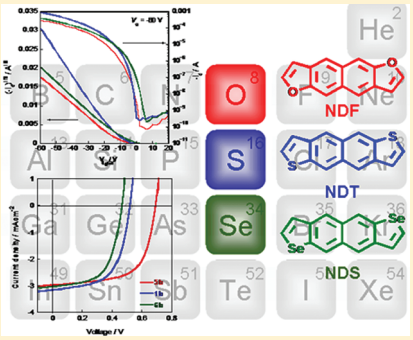

KEYWORDS: *naphthodichalcogenophene, electronic structure, organic semiconductor, organic field-effect transistor, organic photovoltaic*

INTRODUCTION

Recent interests in organic electronics are motivated by their potential applications that can provide low-cost, large-area electronic devices on arbitrary substrates.[1] One of the key materials in organic electronics is, needless to say, the organic semiconductor, which has been recently developed significantly; tuning the chemical structures and physical properties and understanding the structural implications of electronic properties have been intensively studied in the past decade.[2] Among the numbers of molecular classes reported so far, ladder-type π-conjugated molecules, often referred as acenes and heteroacenes have been examined as promising organic semiconductors, which, in fact, have realized high-performance organic field-effect transistors (OFETs)[3] and organic photovoltaics (OPVs).[4]

Acenedithiophenes (AcDTs), such as benzo[1,2-*b*:4,5-*b*′]-dithiophene (BDT) and anthra[2,3-*b*:6,7(7,6)-*b*′]dithiophenes (ADT) (Figure 1), are prototypical of such heteroacenes and have been widely utilized as important π-cores for the development of not only molecular organic semiconductors but also polymer semiconductors.[5] Recently, we reported on the syntheses, characterization, and utilization of four isomeric naphthodithiophenes (NDTs, Figure 1)[6] as new members in AcDTs and found that NDTs are very useful as superior π-extended cores for molecular semiconductors as well as polymer semiconductors.[7] In particular, the linear-shaped

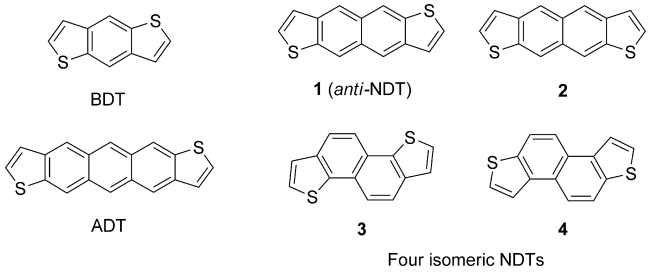

Figure 1. Molecular structures of linear-shaped acenedithiophenes (AcDTs) and four isomeric naphthodithiophenes (NDTs).

naphtho[2,3-*b*:6,7-*b*′]dithiophene (*anti*-NDT, **1**) is a promising one, whose diphenyl derivative afforded OFETs with high mobility of up to 1.5 $cm^2\ V^{-1}\ s^{-1}$.[6b] Furthermore, very recently Facchetti and co-workers have reported that its dialkyloxy derivatives carrying two thiophene-capped diketopyrrolopyrroles (TDPP) showed remarkable results on bulk-heterojunction organic photovoltaics (OPVs) with power conversion efficiencies higher than 4.0%.[8]

Received: September 21, 2011
Revised: November 24, 2011
Published: November 26, 2011

dx.doi.org/10.1021/cm202853b | *Chem. Mater.* 2012, 24, 190–198

These promising results on the *anti*-NDT core have indeed propelled us to study its homologues with different chalcogene atoms,[9,10] that is, naphtho[2,3-*b*:6,7-*b*′]difurans (NDFs, **5**) and naphtho[2,3-*b*:6,7-*b*′]diselenophenes (NDSs, **6**) (Figure 2). In this paper, we report the facile synthesis and properties of these new naphthodichalcogenophenes (NDXs) together with OFET and OPV devices using their diphenyl derivatives (DPh-NDXs).

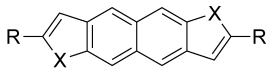

X = O: R = H (NDF, **5a**), R = Ph (DPh-NDF, **5b**)
X = S: R = H (NDT, **1a**), R = Ph (DPh-NDT, **1b**)
X = Se: R = H (NDS, **6a**), R = Ph (DPh-NDS, **6b**)

Figure 2. Molecular structures of naphtho[2,3-*b*:6,7-*b*′]-dichalcogenophenes (NDXs).

RESULTS AND DISCUSSION

Synthesis. A key intermediate in the syntheses of both NDFs (**5**) and NDSs (**6**) is 3,7-dibromo-2,6-dihydroxynaphthalene (**7**), conveniently prepared from 2,6-dihydroxynaphthalene via bromination and selective debromination.[6b] The bromine and hydroxyl functionalities on **7**, however, play different roles in the respective synthesis. For the synthesis of NDF derivatives, the bromine atoms were first replaced with acetylene moieties by the Sonogashira reaction after acetylation on the hydroxyl moieties. Then, the subsequent base-promoted furan formation[11] at the acetyl-protected *o*-ethynylphenol substructures readily gave NDF derivatives in acceptable yields for both the parent compound (**5a**) and the diphenyl derivative (**5b**) (Scheme 1).

For the synthesis of NDSs, on the other hand, the hydroxyl groups were utilized as the handle for introducing the acetylene moieties via triflation and the subsequent chemo-selective Sonogashira coupling to give 3,7-dibromo-2,6-diethynylnaphthalenes (**11**).[6b] Selenophene ring annulation was achieved by a reaction with sodium selenide reagent, in situ generated from sodium borohydride and selenium powder in ethanol, where the first S_NAr-type reaction on the bromine sites to afford *o*-ethynylselenolate intermediates, which then cyclized intramolecularly to give the NDS derivatives.[12] Parent **5a** and **6a** were fully characterized by spectroscopic analyses, whereas the diphenyl derivatives (**5b** and **6b**) do not have solubilities sufficient for the characterization by NMR spectroscopy and thus were characterized by mass spectroscopy and combustion elemental analyses.

Physicochemical Properties. Electrochemical and optical behaviors of **5a** and **6a** along with NDT (**1a**)[6b] were compared to evaluate the influence of the chalcogenophene rings on the molecular properties. At the first glance, the cyclic voltammograms (CVs) of three compounds (Figure 3a) present two noticeable features; their similar oxidation onset potentials and irreversibility of the **5a** voltammogram in contrast to the reversible voltammograms of **1a** and **6a**. Similar oxidation onsets strongly imply that these compounds have similar highest occupied molecular orbital (HOMO) energy levels. Under the premise that the Fc/Fc^+ redox couple corresponds to 4.8 eV below the vacuum level,[13] the HOMO energy levels estimated from the oxidation onsets are 5.5, 5.3, and 5.3 eV for **5a**, **1a**, and **6a**, respectively, which are also close to the formal isoelectronic hydrocarbon, naphthacene (5.2 eV determined by the same procedure). These experimentally estimated HOMO energy levels qualitatively agree with those of theoretically calculated ones (Figure 4),[14] where a slightly low-lying HOMO energy level for **5a** compared to those of **1a** and **6a** is reproduced. On the other hand, the irreversible redox wave of **5a** is markedly contrasted to the reversible voltammograms of **1a** and **6a** (Figure 3a). Repeated redox cycles of **5a** gradually reduced the intensity of the oxidation peak without emergence of new peaks in the voltamogram, indicating that the oxidized species of **5a** seems to be decomposed under the voltammetric conditions. In fact, dark-colored insoluble material was deposited on the surface of the working electrode.

Absorption spectra of **5a**, **1a**, and **6a** depicted in Figure 3b also demonstrate marked electronic-structure difference between **5a** and **1a**/**6a** and similarity of **1a** and **6a**. These difference and similarity can be qualitatively understood by their aromatictiy and effectiveness of π-delocalization over the naphthodichalcogenophene cores. Furan is known as the least aromatic among the present three heteroaromatics,[15] indicating its poor conjugation nature. This can lead to the least effective π-delocalization over the entire 18-π electron system of **5a** core, resulting in the blue-shifted absorption band among the three compounds. In other words, the electronic structures of **1a** and **6a** are somehow similar to that of naphthacene, whereas that of **5a** can be, to some extent, expressed as an oxygen-bridged divinylnaphthalene. The theoretical TD-DFT calculations also reproduce the blue-shifted absorption of **5a** compared to those

Scheme 1. Synthesis of NDF (5) and NDS (6) Derivatives

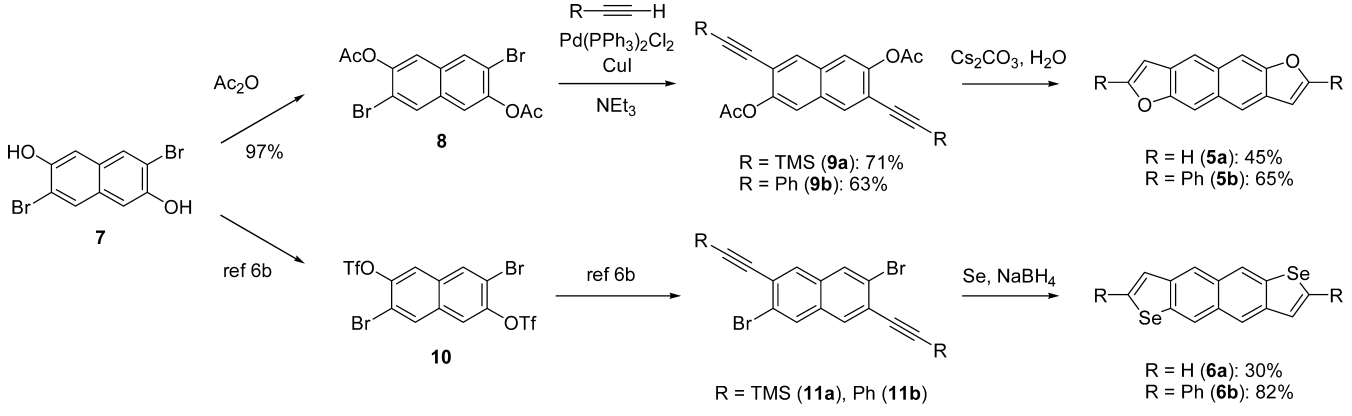

dx.doi.org/10.1021/cm202853b | *Chem. Mater.* 2012, 24, 190–198

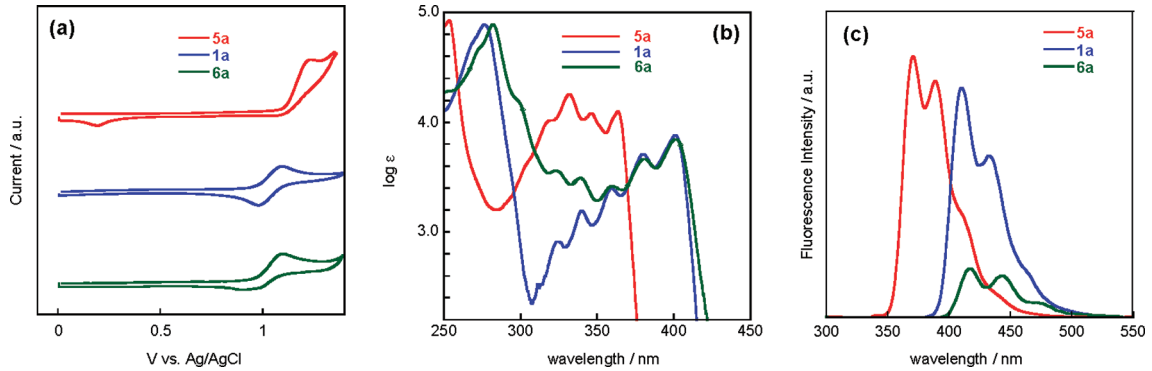

Figure 3. Cyclic voltammogram (a), absorption spectra (in dichloromethane) (b) and fluorescence spectra (λ_{ex} = 254, 276, 282 nm, respectively) (c) of **5a**, **1a**, and **6a**.

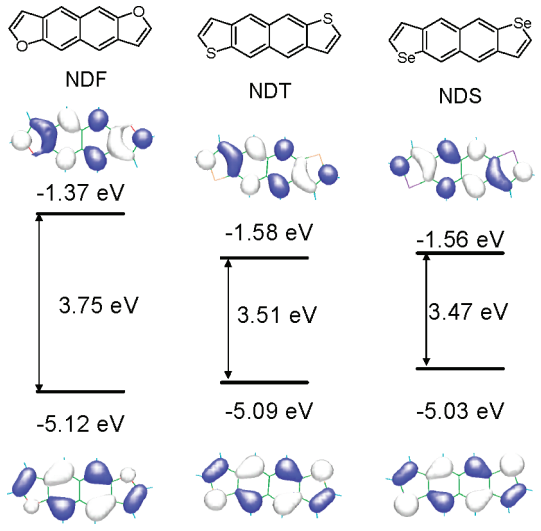

Figure 4. Calculated HOMOs and LUMOs of **5a**, **1a**, and **6a** with the DFT B3LYP/6-31(d) level. The electronic transition energies are also calculated with the TD-DFT B3LYP/6-31(d) level to be 3.47 (**5a**), 3.17 (**1a**), and 3.10 eV (**6a**).

of **1a** and **6a**; the calculated electronic transition energies for **5a**, **1a**, and **6a** are 3.47, 3.17, and 3.10 eV, respectively (Supporting Information, Table S1). Fluorescence spectra of **5a**, **1a**, and **6a** are also depicted in Figure 3c. Similar to the absorption spectra, the furan analogue (**5a**) shows the most blue-shifted emission band among the three analogues. On the other hand, the selenophene analogue (**6a**) has markedly reduced emission intensity compared to those of **5a** and **1a**, which can be understood by considering the heavy atom quenching effect of the incorporated selenium atom.[16]

Thin Film of Diphenyl Derivatives and Their Applications to OFETs and OPVs. *Thin Film Characterizations.* As the film-forming natures of parent **5a** and **6a** were rather poor under typical vacuum deposition conditions, we took the diphenyl derivatives (**5b**, **6b**) to examine the utility of NDF and NDS as an organic semiconducting core in comparison to **1b** previously reported.[6b] All the three compounds afforded homogeneous thin films both on Si/SiO_2 and ITO substrates. Atomic force microscope (AFM) images of the evaporated thin films of **5b**, **1b**, and **6b** on the ITO substrates shown in Figure 5 revealed that all the films consist of crystalline grains with submicrometer in size as seen in typical vapor-deposited thin-films of molecular semiconductors. Although the grain sizes were somewhat different, the surface morphologies of the evaporated thin films on the Si/SiO_2 substrates were basically the same with those on the ITO substrate (Supporting Information, Figure S1).

To evaluate the electronic properties of the thin films, we first measured the ionization potentials (IP) of the evaporated thin films by photoelectron spectroscopy in air (Figure 6a). The IPs of **1b** and **6b** are almost the same (~5.2 eV), whereas that of **5b** is slightly larger (5.4 eV), which can be explained by the inherent difference of the HOMO energy levels of the core parts (see Figure 3a, Figure 4, and Table 1). Although the IPs are somewhat different, all these materials are expected to be stable p-channel organic semiconductors in air owing to their relatively low-lying HOMO energy levels.

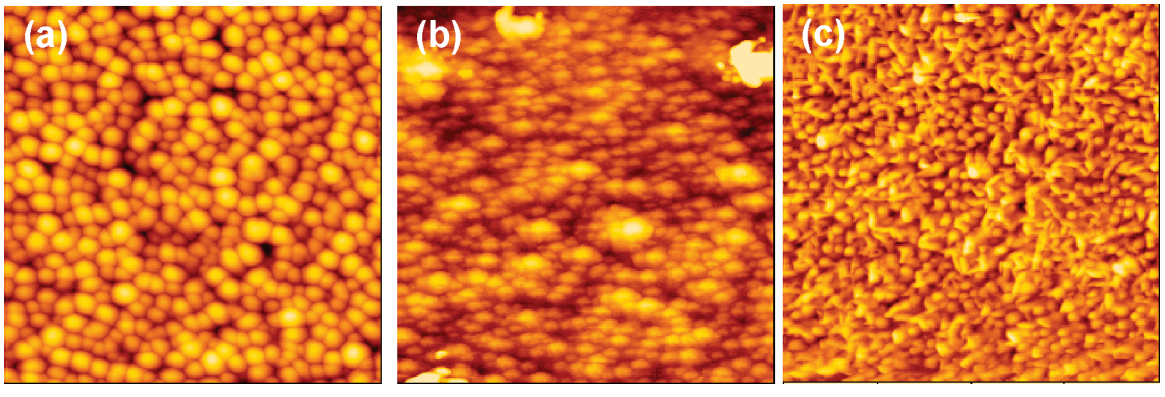

Figure 5. AFM images (2 × 2 μm) of evaporated thin films of **5b** (a), **1b** (b), and **6b** (c) on ITO substrates.

dx.doi.org/10.1021/cm202853b | *Chem. Mater.* 2012, 24, 190–198

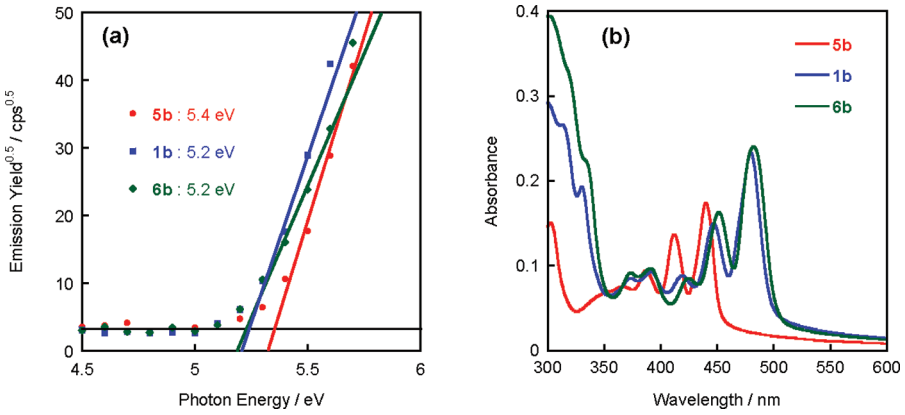

Figure 6. Photoelectron spectroscopy in air (a) and absorption spectra of evaporated thin films (b) of **5b**, **1b**, and **6b** on ITO substrates.

Table 1. Electronic Properties of 5a, 1a, and 6a

compound	E_{onset}/V[a]	HOMO/eV[b]	λ_{max} (λ_{edge})/nm	E_g/eV[c]	λ_{em}/nm[d]	ϕ_{em} [e]
5a	+1.14	−5.5	364 (370)	3.4	370, 390	0.18
1a	+0.94	−5.3	401 (410)	3.0	410, 433	0.10
6a	+0.94	−5.3	401 (410)	3.0	418, 444	8.3×10^{-3}

[a]V vs Ag/AgCl. All the potentials were calibrated with the Fc/Fc$^+$ ($E^{1/2}$ = +0.43 V measured under identical conditions). [b]Estimated with a following equation: E^{HOMO} (eV) = −4.4 − E_{onset}. [c]Calculated from λ_{edge}. [d]Excited at 256, 277, and 282 nm for **5a**, **1a**, and **6a** respectively. [e]Emission quantum yields were determined by the relative method using anthracene (ϕ_{em} 0.31, for **5a**) and 9,10-diphenylanthoracene (ϕ_{em} 0.90, for **1a** and **6a**) as the standards.

The absorption spectra of the thin films have a similar trend with the solution absorption spectra of their heteroacene cores (Figure 6b); very similar absorption bands for **1b** and **6b** and a distinctly blue-shifted absorption for **5b** are observed. These similarity/difference between the thin films are well understood in terms of the molecular electronic structure of the heteroacene core as already discussed.

Both out-of-plane and in-plane X-ray diffraction (XRD) patterns of the evaporated thin films (Figure 7) clearly indicate that the films are nicely crystalline on both the Si/SiO_2 and the ITO substrates (Supporting Information, Figure S2). From the out-of-plane XRD patterns, it can be determined that all three material have edge-on molecular orientations with molecular lamellar structures in the thin film state, and the interlayer spacings (*d*-spacings, 20.2−20.8 Å) calculated from the out-of-plane patterns are close to the molecular lengths expected from theoretically optimized molecular geometries (Supporting Information, Figure S3).

As all the peaks observed in the XRD patterns of the **1b** thin film are indexed by using the bulk single crystallographic cell previously reported[6b] (Figure 7b), **1b** must have basically the same packing structure in both the bulk crystal and the thin film. More precisely, the **1b** crystallites in the thin film have a preferred orientation, where the crystallographic *c*-axis stands perpendicular to the substrate surface and the crystallographic *ab*-plane lies on the substrate surface. This orientation can afford a two-dimensional (2D) electronic structure on the substrate surface, originating from the isotropic herringbone molecular arrangement in the in-plane direction. It is well-known that such structural type is desirable for effective carrier transport in the OFET devices, as the 2D electronic structure on the substrate surface enables isotropic and effective carrier transport leading to high carrier mobility.[17] In fact, this consideration is consistent with the high carrier mobility (1.5 $cm^2\ V^{-1}\ s^{-1}$) of **1b**-based thin film OFET devices.[6b]

Although the single crystals suitable for X-ray structural analyses were not obtained for **5b** and **6b**, it is likely expected, judging from both the out-of-plane and the in-plane XRD patterns (Figure 7a and 7c), that their molecular ordering manner in the thin film state is similar to that of **1b** with the edge-on molecular orientation and good crystalline order in the in-plane direction. Thus, the **5b** and **6b** thin films are also expected as superior semiconducting channel in the OFETs devices (vide infra).

Thin Film OFETs. OFETs of **5b** and **6b** were fabricated using the thin films deposited on the Si/SiO_2 substrates modified with hexamethyldisilazane (HMDS) or octyltrichlorosilane (OTS). Although the transistor characteristics were affected by the fabrication conditions such as the surface treatment and substrate temperature during film deposition, their OFETs in general showed typical p-channel transistor characteristics with mobility higher than 0.1 $cm^2\ V^{-1}\ s^{-1}$ in air (Supporting Information, Table S2). Typical output and transfer curves of the OFETs are depicted in Figure 8, and optimized FET characteristics are summarized in Table 2. The mobilities of the optimized OFETs of **5b** and **6b** are 0.6 and 0.9 $cm^2\ V^{-1}\ s^{-1}$, respectively, which are slightly lower than those previously reported for **1b**-based OFETs (1.5 $cm^2\ V^{-1}\ s^{-1}$).[6b] Relatively low mobility of **5b**- and **6b**-based OFETs can be attributed to the miss-oriented grains as observed in the XRD patterns. In the case of **1b** thin films, no detectable peaks originated from the face-on orientation, that is, the in-plane peaks (110, 120, and 020) in the out-of-plane XRD pattern (Figure 7b) is observed, whereas the out-of-plane XRDs for both **5b** and **6b** have noticeable peaks assignable to the in-plane peaks designated with red asterisks (Figure 7a and 7c). These miss-oriented crystal grains can be a cause for carrier traps that limit experimental carrier mobility. Although the reasons for such miss-orientation for the **5b** and **6b** thin films are not clear, we speculated that the size of chalcogenophene rings attached on the naphthalene can play an important role; the molecular

dx.doi.org/10.1021/cm202853b | *Chem. Mater.* 2012, 24, 190−198

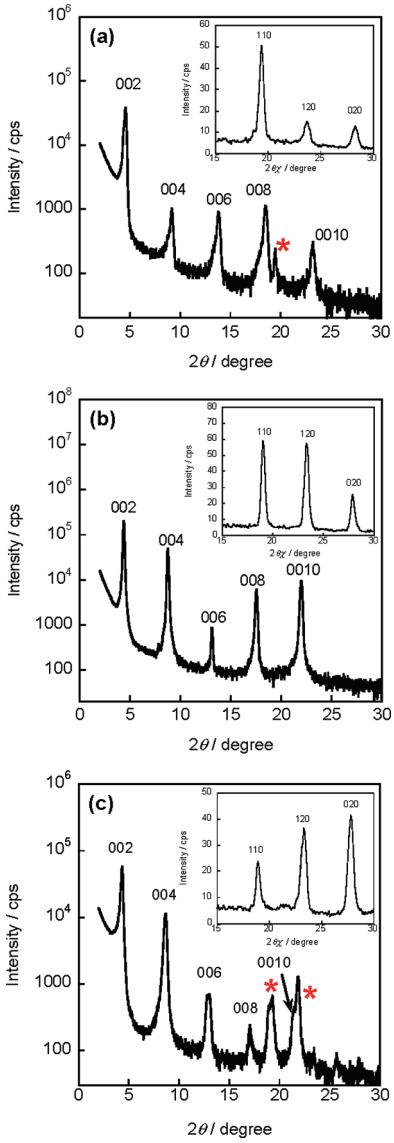

Figure 7. Out-of-plane and in-plane (insets) XRD patterns of evaporated thin films of (a) **5b**, (b) **1b**, and (c) **6b** on Si/SiO_2 substrates.

shape of the present materials is almost straight and rectangular, but the size of the chalcogenophene rings can slightly alter the molecular shape that may affect overall packing effectiveness, resulting in different crystallinity for the three compounds; the oxygen atoms in furan rings in **5b** could intrude from the edge of the rectangular shaped molecule, whereas the selenium atoms in **6b** protrude vice versa.

Several furan-based materials, including α-oligofurans, furan-thiophene co-oligomers, and furan-including donor–acceptor type polymers, have been applied as an active semiconducting material in OFET devices.[18] Some of these materials show promising device characteristics with high mobility,[18c,e] indicating the great potential of furan as a substructure for electronic materials. The present results on the **5b**-based OFETs can be another example of a superior furan-based material, and thus, it can be said that the fused-furan structure is also a promising substructure in the development of new organic semiconductors for transistor applications. On the other hand, selenophene-incorporated materials have been also investigated with expectation that extended molecular orbitals brought about by selenium atoms are beneficial for effective intermolecular orbital couplings in the solid state, which might enhance carrier mobility.[10,19] In the present study, however, such positive effect is not the case, instead, perturbation to packing perfection in the thin film state seems to limit the carrier mobility in the actual thin film OFETs.

Bilayer OPVs. Standard donor/acceptor (D/A) bilayer solar cells with a device structure of ITO/DPh-NDXs/C_{60}/BCP/Al were fabricated by using sequential vacuum depositions on ITO-coated glass substrates.[20] Current density–voltage (*J-V*) characteristics of devices were measured under simulated AM 1.5 G solar illumination (100 mW cm^{-2}) in air without encapsulation. All the devices showed typical photovoltaic responses as shown in Figure 9a. Reflecting the relatively narrow absorption ranges of the thin films (Figure 6b), short-circuit currents (J_{sc}'s) are not that large (~ 3 mA cm^{-2}) regardless of the donor layer: in fact external quantum efficiency (EQE) spectra (Figure 9b) of the devices indicate that there is almost no photocurrent response above 650 nm. In sharp contrast to similar J_{sc}'s, open circuit voltage (V_{oc}) depends largely on the donor material; as expected from the larger IP, in other words, lower HOMO energy level, of **5b** (5.4 eV) than those of **1b** and **6b** (5.2 eV), the **5b**-based devices afforded larger V_{oc} (0.69 V) by about 0.2 V. Another noticeable feature of the current OPVs is fairly good fill factors (*FF*s, 0.59–0.64). This could be partially attributed to slower charge-recombination (CR) rate,[21] expected from the structure at the D/A interface, where the perpendicular orientation of the donors against C_{60} molecules originating from the edge-on structure of the donor molecules on the substrate is most likely. As a result, the **5b**-based devices showed the best power conversion efficiency (PCE) of 1.31%, which is relatively good for simple bilayer solar cells based on small-molecular based OPVs.[22]

The deep HOMO energy levels of DPh-NDXs (~5.4 eV) affording large V_{oc}'s (~0.69 V) and their large HOMO–LUMO gaps limiting their photoharvesting ability in the visible range leading to low J_{sc}'s (~3.16 mA cm^{-2}) are indeed an unavoidable two-sidedness as the donor materials for OPV applications. To compensate the limited photoharvesting nature, we utilized C_{70} having a better light absorption property than that of C_{60}[23] as the electron accepting layer in **5b**-based OPVs. Figure 10a shows the absorption and EQE spectra the **5b**/C_{70} bilayer film, which shows much enhanced light absorption and better EQE in the visible range as expected. As a result, fairly enhanced J_{sc} (~4.59 mA) keeping high V_{oc} (~0.69 V) and *FF* (~0.63) was achieved, resulting in an overall PCE of 2.0% (Figure 10b).

■ CONCLUSION

In summary, we have successfully synthesized a series of linear-shaped naphthodichalcogenophenes and evaluated them as organic semiconductors. In their synthesis, 3,7-dibromo-2,6-dihydroxynaphthalene (**7**) was a versatile key intermediate for both the NDF and the NDS derivatives, although the roles of the bromine and hydroxyl groups are different. Comparison of physicochemical properties of **5a**, **1a**, and **6a** clearly showed similarities of **1a** and **6a**, and differences between **5a** and **1a**/**6a**. These trends in the molecular properties are basically understood by the lower aromaticity of furan compared to those of thiophene and selenophene. On the other hand, the FET characteristics of the vapor-deposited DPh-NDXs devices were almost similar to one another; the field-effect mobilties extracted from the saturation regime are only slightly lower for **5b**- and **6b**-based devices than that of **1b**-based one. The

dx.doi.org/10.1021/cm202853b | *Chem. Mater.* 2012, 24, 190–198

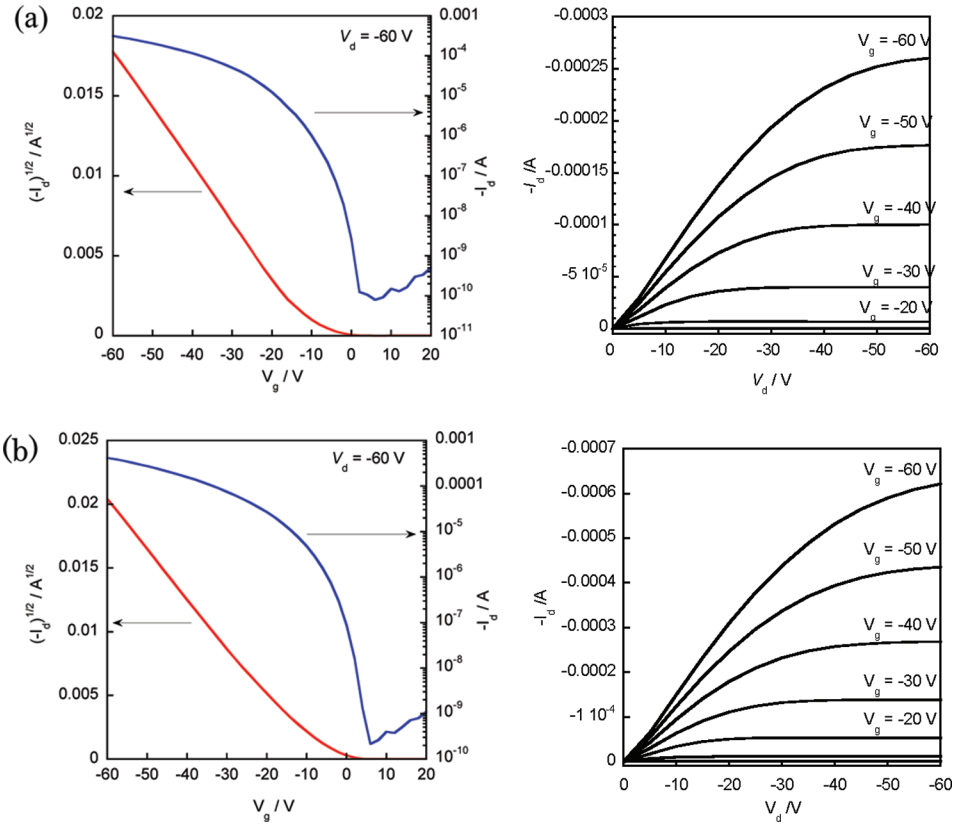

Figure 8. Output and transfer characteristics of FETs fabricated on OTS-treated Si/SiO_2 substrate: (a) **5b** (T_{sub} = 100 °C), (b) **6b** (T_{sub} = 100 °C).

Table 2. Characterization of Evaporated Thin Films, OFET and OPV[a] Devices of 5b, 1b, and 6b

compound	IP[b]/eV	λ_{max} (λ_{edge})/nm	E_g[c]/eV	μ_{FET}[d]/cm^2 V^{-1} s^{-1}	J_{sc}/mA cm^{-2}	V_{oc}/V	*FF*	η/%
5b	5.4	440 (464)	2.67	0.6	2.98	0.69	0.64	1.31
1b	5.2	480 (514)	2.41	1.5[e]	3.16	0.52	0.60	0.98
6b	5.2	482 (512)	2.42	0.9	3.03	0.46	0.59	0.83

[a]Obtained by using typical bilayer OPVs with a device structure of ITO/donor/C_{60}/BCP/Al under AM 1.5 G solar simulator (100 mW cm^{-2}) illumination. [b]Determined by photoemission yield spectroscopy in air. [c]Estimated from absorption edge. [d]Extracted from the saturation regime for the optimized devices. [e]Reference 6b.

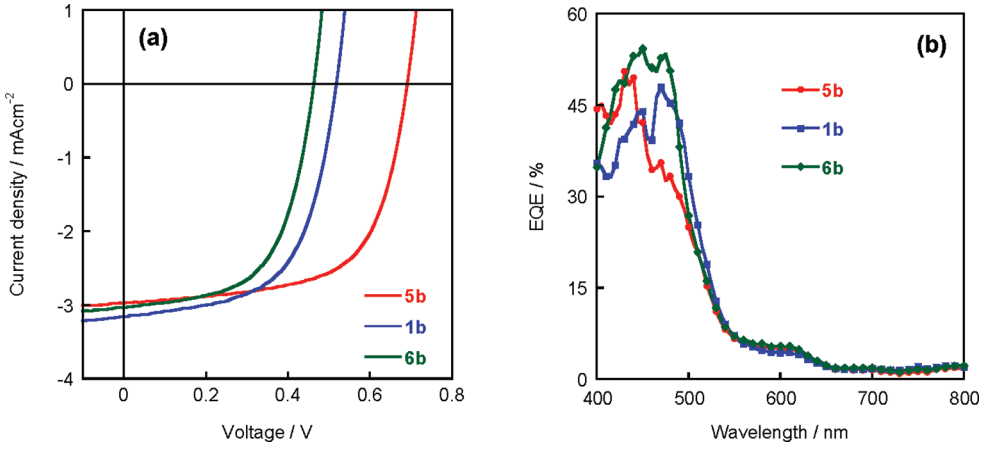

Figure 9. *J-V* characteristics under AM 1.5 G solar simulator (100 mW cm^{-2}) illumination (a) and EQE spectra of ITO/donor/C_{60}/BCP/Al solar cell (b).

reduced mobilities for the former can mostly be attributed to miss-oriented molecular ordering in the thin film state elucidated by thin film XRD measurements. The DPh-NDX/C_{60} bilayer films acted as a photoactive interface showing typical OPV characteristics. Among them, the **5b**-based OPV showed the highest PCE of 1.31%, mainly owing to its large V_{oc} (0.69 V), originating from its low-lying HOMO energy level. Although its large HOMO−LUMO gap makes its thin-films

dx.doi.org/10.1021/cm202853b | *Chem. Mater.* 2012, 24, 190−198

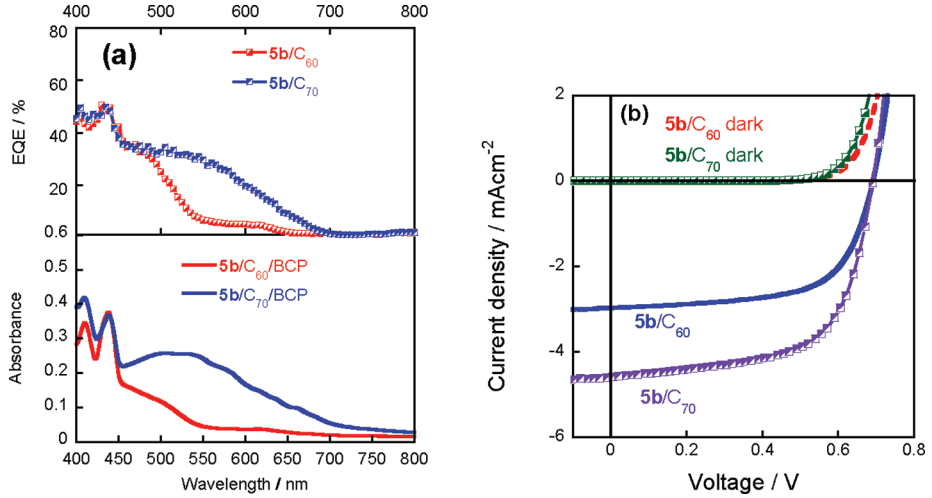

Figure 10. Absorption spectra of **5b**/C_{70} bilayer film and EQE spectra of the **5b**/C_{70}/BCP solar cell (a) and *J-V* characteristics of the solar cell under AM 1.5 G solar simulator (100 mW cm^{-2}) illumination (b).

transparent in the visible range resulting in limited J_{sc} in the bilayer OPVs, its capability to afford relatively large V_{oc} is advantageous; the combination with C_{70} as an accepting layer enables improved OPV performances with a PCE of 2.0%. These results clearly indicated that fused-furan substructures are also a useful structural motif in developing electronic materials for opto/electronic applications such as OFETs and OPVs. In particular, molecular modifications on the NDF core that allow smaller HOMO−LUMO gap to improve photo absorption property while keeping the low-lying HOMO energy level are the next issue for making further use of the advantages of the NDF core.

EXPERIMENTAL SECTION

Synthesis. *General Procedures.* All chemicals and solvents were of reagent grade unless otherwise indicated. THF and NMP were purified with a standard procedure prior to use. 3,7-Dibromo-2,6-dihydroxynaphthalene (**7**), 3,7-dibromo-2,6-bis-(trifluoromethanesulfonyloxy)naphthalene (**10**), 2,6-dibromo-3,7-bis-(trimethylsilylethynyl)naphthalene (**11a**), and 2,6-dibromo-3,7-bis-(phenylethynyl)naphthalene (**11b**) were synthesized as reported.[6b] Melting points were uncorrected. All reactions were carried out under nitrogen atmosphere. Nuclear magnetic resonance spectra were obtained in deuterated chloroform ($CDCl_3$) with TMS as internal reference unless otherwise stated; chemical shifts (δ) are reported in parts per million. IR spectra were recorded using a KBr pellet for solid samples. EI-MS spectra were obtained using an electron impact ionization procedure (70 eV). The molecular ion peaks of the chlorine, bromine, or selenium containing compounds showed a typical isotopic pattern, and all the mass peaks are reported based on ^{79}Br or ^{80}Se, respectively.

*2,6-Diacetoxy-3,7-dibromonaphthalene (**8**).* To a suspension of 2,6-dibromo-3,7-dihydroxynaphthalene (7, 31.8 g, 0.10 mol) and pyridine (20 mL, 0.21 mol) in CH_2Cl_2 (300 mL) was added acetic anhydride (50 mL, 0.60 mol) at room temperature (rt). After the mixture was stirred for 15 h at the same temperature, diluted hydrochloric acid (1M, 100 mL) was added. The resulting mixture was separated, and the aqueous layer was extracted with dichloromethane (100 mL × 2). The combined organic layer was dried ($MgSO_4$) and concentrated in vacuo, and the resulting residue was purified by column chromatography on silica-gel eluted with chloroform (R_f 0.5) to give **8** (39.2 g, 97%) as a white solid. Mp 266.5−267.1 °C;^1H NMR (400 MHz, $CDCl_3$) δ 2.41, (s, 6H), 7.52 (s, 2H), 8.06 (s, 2H); ^{13}C NMR (100 MHz, $CDCl_3$) δ 168.7, 146.1, 131.9, 131.6, 120.0, 116.8, 20.8; EIMS (70 eV) m/z = 400 (M^+); IR (KBr) ν = 1747 (C═O) cm^{-1}; Anal. Calcd for $C_{14}H_{10}Br_2O_4$: C, 41.84; H, 2.51%. Found: C, 42.14; H, 2.41%.

*2,6-Diacetoxy-3,7-bis(trimethylsilylethynyl)naphthalene (**9a**).* To a deaerated solution of **8** (2.0 g, 5.0 mmol) and diisopropylamine (50 mL) in *N,N*-dimethylacetamide (50 mL) was added $Pd(PPh_3)_2Cl_2$ (350 mg, 0.028 mmol, 10 mol %), CuI (190 mg, 0.056 mmol, 20 mol %), and trimethylsilylacethylene (3.4 mL, 25.0 mmol). After the mixture was stirred for 24 h at 60 °C, water (1 mL) and hydrochloric acid (1M, 100 mL) were subsequently added. The resulting mixture was extracted with chloroform (100 mL × 2), and the combined organic layer was dried ($MgSO_4$) and concentrated in vacuo. The residue was purified by silica-gel column chromatography (eluent, dichloromethane-hexane, 1:1 v/v) and recrystallization from chloroform-ethyl acetate to give **9a** (1.55 g, 71%) as a white solid. Mp 215.0−215.8 °C; ^1H NMR (400 MHz, $CDCl_3$) δ 0.27 (s, 18H), 2.37 (s, 6H), 7.46 (s, 2H), 7.93 (s, 2H); ^{13}C NMR (100 MHz, $CDCl_3$) δ 169.0, 148.9, 133.2, 131.1, 119.3, 118.1, 101.1, 99.7, 21.0, 0.2; EIMS (70 eV) m/z = 436 (M^+); IR (KBr) ν = 2154 (acetylene), 1769 (C═O) cm^{-1}; Anal. Calcd for $C_{24}H_{28}O_4Si_2$: C, 66.02; H, 6.46%. Found: C, 65.91; H, 6.73%.

*2,6-Diacetoxy-3,7-bis(phenylethynyl)naphthalene (**9b**).* A similar procedure as above using ethynylbenzene gave the title compound in 63% isolated yield. Mp 250.1−250.6 °C;^1H NMR (400 MHz, $CDCl_3$) δ 2.43 (s, 6H), 7.37−7.40 (m, 6H), 7.52−7.55 (m, 4H), 7.56 (s, 2H), 8.03 (s, 2H); ^{13}C NMR (100 MHz, $CDCl_3$) δ 169.2, 148.7, 132.7, 131.8, 129.0, 128.7, 122.8, 119.4, 118.2, 95.3, 84.6, 21.1; EIMS (70 eV) m/z = 444 (M^+); IR (KBr) ν = 1768 (C═O) cm^{-1}; Anal; Calcd for $C_{30}H_{24}O_4$: C, 81.07; H, 4.54%. Found: C, 80.86; H, 4.30%.

*Naphtho[2,3-b:6,7-b′]difuran (**5a**).* To a solution of **9a** (0.3 g, 0.688 mmol) in *N,N*-dimethylacetamide (10 mL) and water (2 mL) was added Cs_2CO_3 (2.05 g, 6.88 mmol). After the mixture was stirred at 80 °C for 24 h, water (20 mL) was added. The resulting mixture was extracted with dichloromethane (50 mL × 2), and the combined organic layer was dried ($MgSO_4$) and concentrated in vacuo. The residue was purified by silica-gel column chromatography (eluent, hexane) and GPC to give **5a** (145 mg, 45%) as a white solid. Mp 241.5−242.3 °C; ^1H NMR (400 MHz, $CDCl_3$) δ 6.87 (d, J = 2.0 Hz, 2H), 7.72 (d, J = 2.0 Hz, 2H), 8.01 (s, 2H), 8.14 (s, 2H); ^{13}C NMR (100 MHz, $CDCl_3$) δ 153.2, 147.6, 128.8, 128.4, 118.5, 106.6, 106.2; EIMS (70 eV) m/z = 208 (M^+) ; Anal. Calcd for $C_{14}H_8O_2$: C, 80.76; H, 3.87%. Found: C, 80.58; H, 3.79%.

*2,7-Diphenylnaphtho[2,3-b:6,7-b′]difuran (**5b**).* To a solution of **9b** (0.3 g, 0.675 mmol) in *N,N*-dimethylacetamide (10 mL) and water (2 mL) was added Cs_2CO_3 (2.01 g, 6.75 mmol). The mixture was stirred at 80 °C for 24 h and then diluted with water (20 mL). The resulting precipitate was collected by filtration and washed subsequently with water, methanol, and $CHCl_3$ and dried in air. The

dx.doi.org/10.1021/cm202853b | *Chem. Mater.* 2012, 24, 190−198

crude product was purified by vacuum sublimation (source temperature: 240 °C at about 1.0×10^{-3} Pa) to give **5b** (157 mg, 65%) as a yellow solid. Mp >300 °C; EIMS (70 eV) m/z = 360 (M^+); Anal. Calcd for $C_{26}H_{16}O_2$: C, 86.65; H, 4.47%. Found: C, 86.54; H, 4.23%.

*Naphtho[2,3-b:6,7-b′]diselenophene (**6a**).* To a suspension of selenium powder (28 mg, 0.35 mmol) in ethanol (1 mL) was added sodium borohydride ($NaBH_4$, 14 mg, 0.35 mmol) at ice-bath temperature. After the mixture was stirred for 40 min at the same temperature, NMP (5 mL) and 2,6-dibromo-3,7-bis-(trimethylsilylethynyl)naphthalene (**11a**, 50 mg, 0.1 mmol) was added. The mixture was heated at 185 °C with distilling out ethanol using a Dean−Stark condenser for 12 h. After cooling, the mixture was poured into saturated aqueous ammonium chloride solution (10 mL). The resulting precipitate was collected by filtration and purified by vacuum sublimation (source temperature: 190 °C at about 1.0×10^{-3} Pa) to give **6a** (10 mg, 30%) as a white solid. Mp >300 °C; ^{1}H NMR (400 MHz, $CDCl_3$) δ 7.66 (d, J = 5.9 Hz, 2H), 7.98 (d, J = 5.9 Hz, 2H), 8.37 (s, 2H), 8.52 (s, 2H); EIMS (70 eV) m/z = 334 (M^+); Anal. Calcd for $C_{14}H_8Se_2$: C, 81.07; H, 4.54%. Found: C, 80.87; H, 4.30%.

*2,7-Diphenylnaphtho[2,3-b:6,7-b]diselenophene (**6b**).* To a suspension of selenium powder (282 m, 3.5 mmol) in ethanol (8 mL) was added sodium borohydride (136 mg, 3.5 mmol) at ice-bath temperature. After the mixture was stirred for 40 min at the same temperature, NMP (40 mL) and 2,6-dibromo-3,7-bis(phenylethynyl)-naphthalene (**11b**, 486 mg, 1.0 mmol) were added. Then, the mixture was heated at 185 °C with distilling out ethanol using a Dean−Stark trap for 12 h. After cooling, the resulting mixture was poured into a saturated aqueous ammonium chloride solution (50 mL). The resulting precipitate was collected by filtration, washed with water, and dried. Continuous extraction from the solid with boiling chloroform afforded **6b** as a pale yellow solid (398 mg, 82%). For device fabrication, **6b** was further purified by vacuum sublimation (source temperature: 340 °C at about 1.0×10^{-3} Pa). Mp >300 °C; EIMS (70 eV) m/z = 486 (M^+); Anal. Calcd for $C_{26}H_{16}Se_2$: C, 64.21; H, 3.32%. Found: C, 64.40; H, 3.11%.

Fabrication and Evaluation of FET Devices. OFETs were fabricated in a "top-contact" configuration on a heavily doped n^+-Si (100) wafer with a 200 nm thermally grown SiO_2 (C_i = 17.3 nF cm^{-2}). The substrate surfaces were treated with octyltrichlorosilane (OTS) or hexamethyldisilazane (HMDS) as reported previously.[6b] A thin film of DPh-NDXs (**5b** and **6b**) as the active layer was vacuum-deposited on the Si/SiO_2 substrates maintained at various temperatures (T_{sub}) at a rate of 1 Å s^{-1} under a pressure of ~10^{-3} Pa. On top of the organic thin film, gold films (80 nm) as drain and source electrodes were deposited through a shadow mask. For a typical device, the drain-source channel length (L) and width (W) are 50 μm and 1.5 mm, respectively. Characteristics of the OFET devices were measured at room temperature under ambient conditions with a Keithley 4200 semiconducting parameter analyzer. Field-effect mobility (μ_{FET}) was calculated in the saturation regime (V_d = −60 V) of the I_d using the following equation,

$$I_d = C_i \mu_{FET} (W/2L)(V_g - V_{th})^2$$

where C_i is the capacitance of the SiO_2 insulator, and V_g and V_{th} are the gate and threshold voltages, respectively. Current on/off ratio (I_{on}/I_{off}) was determined from the I_d at V_g = 0 V (I_{off}) and V_g = −60 V (I_{on}). The μ_{FET} data reported are typical values from more than 10 different devices.

Fabrication and Evaluation of OPV Devices. Standard bilayer solar cells were fabricated by using sequential vacuum depositions on ITO-coated glass substrates.[21] Twice vacuum sublimed DPh-NDXs (**5b**, **1b** or **6b**), C_{60}, and BCP in our laboratory were used. The ITO substrates (110 nm thickness on glass, sheet registance <20 Ω square^{-1}) were successively washed by ultrasonication in a neutral detergent, deionized water, distilled water, acetone, and isopropanol for 10 min. Then, they were treated with UV ozone for 20 min immediately prior to loading into a vacuum chamber (~3×10^{-3} Pa). Thin films of DPh-NDXs (deposition rate: 1 Å s^{-1}, 40 nm), C_{60} (deposition rate: 2 Å s^{-1}, 30 nm), and BCP (2 Å s^{-1}, 10 nm) were subsequently deposited, and then Al (1 Å s^{-1}, 100 nm) used as the cathode was evaporated through a shadow mask with 2.0 mm diameter openings. Current−voltage (J-V) characteristics of cells were measured under simulated AM 1.5 G solar illumination (Asahi-Bunko Co., Ltd.) in air without encapsulation using a Keithley 2400 source meter. ND filters were used to adjust the light intensity measured with a calibrated broadband optical power meter (Newport Instruments).

The power conversion efficiency (η) was calculated using

$$\eta = (J_{sc} V_{oc} FF)/P_o$$

where V_{oc} is the open circuit voltage, J_{sc} is the short-circuit current density, P_o is the power of the incident light, and FF is the fill factor.

■ ASSOCIATED CONTENT

Supporting Information

Instrumentation for the characterization of compounds, complete entry of reference 14, TD-DFT calculations for **5a**, **1a**, and **6a**, MO calculations for **5b**, **1b**, and **6b**, XRD patterns of thin films of **5b**, **1b**, and **6b** on ITO substrates, AFM images of thin films of **5b**, **1b**, and **6b** on Si/SiO_2 substrates, FET characteristics of **5b** and **6b**, NMR spectra of the synthetic intermediates. This material is available free of charge via the Internet at http://pubs.acs.org.

■ AUTHOR INFORMATION

Corresponding Author

*E-mail: ktakimi@hiroshima-u.ac.jp.

Author Contributions

§These two authors contributed equally to this work.

■ ACKNOWLEDGMENTS

This work was financially supported by Grants-in-Aid for Scientific Research (No. 23245041) from MEXT, Japan and by a Founding Program for World-Leading R&D on Science and Technology (FIRST), Japan. One of the authors (S.S.) is grateful for the research fellowship for young scientists from JSPS.

■ REFERENCES

(1) (a) Rogers, J. A.; Bao, Z.; Katz, H. E.; Dodabalapur, A. In *Thin-Film Transistors*; Kagan, C. R., Andry, P., Eds.; Marcel Dekker: New York, 2003; p 377. (b) *Organic Electronics, Manufacturing and Applications*; Klauk, H., Ed.; Wiley-VCH: Weinheim, Germany, 2006. (c) *Organic Field-Effect Transistors*; Bao, Z., Locklin, J., Eds.; CRC Press: Boca Raton, FL, 2007. (d) Facchetti, A. *Mater. Today* **2007**, *10*, 28−37.

(2) (a) Dimitrakopoulos, C. D.; Malenfant, P. R. L. *Adv. Mater.* **2002**, *14*, 99−117. (b) Murphy, A. R.; Frechet, J. M. J. *Chem. Rev.* **2007**, *107*, 1066−1096. (c) Klauk, H. *Chem. Soc. Rev.* **2010**, *39*, 2643−2666. (d) Facchetti, A. *Chem. Mater.* **2011**, *23*, 733−758.

(3) (a) Anthony, J. E. *Chem. Rev.* **2006**, *106*, 5028−5048. (b) Anthony, J. E. *Angew. Chem., Int. Ed.* **2008**, *47*, 452−483. (c) Takimiya, K.; Shinamura, S.; Osaka, I.; Miyazaki, E. *Adv. Mater.* **2011**, *23*, 4347−4370.

(4) (a) Yoo, S.; Domercq, B.; Kippelen, B. *Appl. Phys. Lett.* **2004**, *85*, 5427−5429. (b) Lloyd, M. T.; Mayer, A. C.; Subramanian, S.; Mourey, D. A.; Herman, D. J.; Bapat, A. V.; Anthony, J. E.; Malliaras, G. G. *J. Am. Chem. Soc.* **2007**, *129*, 9144−9149. (c) Yang, J.; Nguyen, T.-Q. *Org. Electron.* **2007**, *8*, 566−574.

(5) (a) Laquindanum, J. G.; Katz, H. E.; Lovinger, A. J.; Dodabalapur, A. *Adv. Mater.* **1997**, *8*, 36−39. (b) Takimiya, K.; Kunugi, Y.; Konda, Y.; Niihara, N.; Otsubo, T. *J. Am. Chem. Soc.* **2004**, *126*, 5084−5085. (c) Takimiya, K.; Kunugi, Y.; Ebata, H.; Otsubo, T. *Chem. Lett.* **2006**, *35*, 1200−1201. (d) Kashiki, T.; Miyazaki, E.; Takimiya, K. *Chem. Lett.*

2008, *37*, 284−285. (e) Kashiki, T.; Miyazaki, E.; Takimiya, K. *Chem. Lett.* **2009**, *38*, 568−569. (f) Laquindanum, J. G.; Katz, H. E.; Lovinger, A. J. *J. Am. Chem. Soc.* **1998**, *120*, 664−672. (g) Payne, M. M.; Parkin, S. R.; Anthony, J. E.; Kuo, C.-C.; Jackson, T. N. *J. Am. Chem. Soc.* **2005**, *127*, 4986−4987. (h) Dickey, K. C.; Anthony, J. E.; Loo, Y. L. *Adv. Mater.* **2006**, *18*, 1721−1726. (i) Chen, M.-C.; Kim, C.; Chen, S.-Y.; Chiang, Y.-J.; Chung, M.-C.; Facchetti, A.; Marks, T. J. *J. Mater. Chem.* **2008**, *18*, 1029−1036.

(6) (a) Shinamura, S.; Miyazaki, E.; Takimiya, K. *J. Org. Chem.* **2010**, *75*, 1228−1234. (b) Shinamura, S.; Osaka, I.; Miyazaki, E.; Nakao, A.; Yamagishi, M.; Takeya, J.; Takimiya, K. *J. Am. Chem. Soc.* **2011**, *133*, 5024−5035.

(7) (a) Osaka, I.; Abe, T.; Shinamura, S.; Miyazaki, E.; Takimiya, K. *J. Am. Chem. Soc.* **2010**, *132*, 5000−5001. (b) Osaka, I.; Abe, T.; Shinamura, S.; Takimiya, K. *J. Am. Chem. Soc.* **2011**, *133*, 6852−6860.

(8) Loser, S.; Bruns, C. J.; Miyauchi, H.; Ortiz, R. P.; Facchetti, A.; Stupp, S. I.; Marks, T. J. *J. Am. Chem. Soc.* **2011**, *133*, 8142−8145.

(9) (a) Tsuji, H.; Mitsui, C.; Ilies, L.; Sato, Y.; Nakamura, E. *J. Am. Chem. Soc.* **2007**, *129*, 11902−11903. (b) Li, H.; Jiang, P.; Yi, C.; Li, C.; Liu, S.-X.; Tan, S.; Zhao, B.; Braun, J.; Meier, W.; Wandlowski, T.; Decurtins, S. *Macromolecules* **2010**, *43*, 8058−8062.

(10) (a) Takimiya, K.; Kunugi, Y.; Konda, Y.; Ebata, H.; Toyoshima, Y.; Otsubo, T. *J. Am. Chem. Soc.* **2006**, *128*, 3044−3050. (b) Izawa, T.; Miyazaki, E.; Takimiya, K. *Chem. Mater.* **2009**, *21*, 903−912. (c) Mishra, S. P.; Javier, A. E.; Zhang, R.; Liu, J.; Belot, J. A.; Osaka, I.; McCullough, R. D. *J. Mater. Chem.* **2011**, *21*, 1551−1561.

(11) (a) Dai, W.-M.; Lai, K. W. *Tetrahedron Lett.* **2002**, *43*, 9377−9380. (b) Hayashi, N.; Saito, Y.; Higuchi, H.; Suzuki, K. *J. Phys. Chem. A* **2009**, *113*, 5342−5347.

(12) Kashiki, T.; Shinamura, S.; Kohara, M.; Miyazaki, E.; Takimiya, K.; Ikeda, M.; Kuwabara, H. *Org. Lett.* **2009**, *11*, 2473−2475.

(13) (a) Pommerehne, J.; Vestweber, H.; Guss, W.; Mahrt, R. F.; Bässler, H.; Porsch, M.; Daub, J. *Adv. Mater.* **1995**, *7*, 551−554. (b) Johansson, T.; Mammo, W.; Svensson, M.; Andersson, M. R.; Inganas, O. *J. Mater. Chem.* **2003**, *13*, 1316−1323. (c) Cardona, C. M.; Li, W.; Kaifer, A. E.; Stockdale, D.; Bazan, G. C. *Adv. Mater.* **2011**, *23*, 2367−2371.

(14) MO calculations were carried out with the DFT/TD-DFT method at the B3LYP/6-31g(d) level using Gaussian 03 program package. Frisch, M. J. et al. *Gaussian 03*, revision C.02; Gaussian, Inc.: Wallingford, CT, 2004.

(15) (a) Cordell, F. R.; Boggs, J. E. *J. Mol. Structure: THEOCHEM* **1981**, *85*, 163−178. (b) Juric, A.; Sabljic, A.; Trinajstic, N. *J. Heterocycl. Chem.* **1984**, *21*, 273−282.

(16) Yang, R.; Tian, R.; Hou, Q.; Zhang, Y.; Li, Y.; Yang, W.; Zhang, C.; Cao, Y. *J. Polym. Sci., Part A: Polym. Chem.* **2005**, *43*, 823−836.

(17) (a) Brédas, J.-L.; Beljonne, D.; Coropceanu, V.; Cornil, J. *Chem. Rev.* **2004**, *104*, 4971−5004. (b) Coropceanu, V.; Cornil, J.; da Silva Filho, D. A.; Olivier, Y.; Silbey, R.; Brédas, J.-L. *Chem. Rev.* **2007**, *107*, 926−952.

(18) (a) Miyata, Y.; Terayama, M.; Minari, T.; Nishinaga, T.; Nemoto, T.; Isoda, S.; Komatsu, K. *Chem.—Asian J.* **2007**, *2*, 1492−1504. (b) Bijleveld, J. C.; Karsten, B. P.; Mathijssen, S. G. J.; Wienk, M. M.; de Leeuw, D. M.; Janssen, R. A. J. *J. Mater. Chem.* **2011**, *21*, 1600−1606. (c) Li, Y.; Sonar, P.; Singh, S. P.; Zeng, W.; Soh, M. S. *J. Mater.* **2011**, *21*, 10829−10835. (d) Gidron, O.; Diskin-Posner, Y.; Bendikov, M. *J. Am. Chem. Soc.* **2010**, *132*, 2148−2150. (e) Gidron, O.; Dadvand, A.; Sheynin, Y.; Bendikov, M.; Perepichka, D. F. *Chem. Commun.* **2011**, *47*, 1976−1978.

(19) (a) Kunugi, Y.; Takimiya, K.; Yamane, K.; Yamashita, K.; Aso, Y.; Otsubo, T. *Chem. Mater.* **2003**, *15*, 6−7. (b) Heeney, M.; Zhang, W.; Crouch, D. J.; Chabinyc, M. L.; Gordeyev, S.; Hamilton, R.; Higgins, S. J.; McCulloch, I.; Skabara, P. J.; Sparrowe, D.; Tierney, S. *Chem. Commun.* **2007**, 5061−5063. (c) Ha, J. S.; Kim, K. H.; Choi, D. H. *J. Am. Chem. Soc.* **2011**, *133*, 10364−10367. (d) Al-Hashimi, M.; Baklar, M. A.; Colleaux, F.; Watkins, S. E.; Anthopoulos, T. D.; Stingelin, N.; Heeney, M. *Macromolecules* **2011**, *44*, 5194−5199.

(20) Tang, C. W. *Appl. Phys. Lett.* **1986**, *48*, 183−185.

(21) Yi, Y.; Coropceanu, V.; Bredas, J.-L. *J. Am. Chem. Soc.* **2009**, *131*, 15777−15783.

(22) (a) Mutolo, K. L.; Mayo, E. I.; Rand, B. P.; Forrest, S. R.; Thompson, M. E. *J. Am. Chem. Soc.* **2006**, *128*, 8108−8109. (b) Kinoshita, Y.; Hasobe, T.; Murata, H. *Appl. Phys. Lett.* **2007**, *91*, 083518. (c) Perez, M. D.; Borek, C.; Forrest, S. R.; Thompson, M. E. *J. Am. Chem. Soc.* **2009**, *131*, 9281−9286. (d) Mori, H.; Takimiya, K. *Appl. Phys. Express* **2011**, *4*, 061602. (e) Brian, E. L.; Guodan, W.; Siyi, W.; Jeramy, D. Z.; Viacheslav, V. D.; Mark, E. T.; Stephen, R. F. *Appl. Phys. Lett.* **2011**, *98*, 243307.

(23) Sakai, J.; Taima, T.; Yamanari, T.; Saito, K. *Sol. Energy Mater. Sol. Cell* **2009**, *93*, 1149−1153.